Optical Engineering

OpticalEngineering.SPIEDigitalLibrary.org

# Adaptive-optic system requirements to mitigate aero-optical aberrations as a function of viewing angle

Shaddy Abado
Stanislav Gordeyev
Eric Jumper

SPIE.

# Adaptive-optic system requirements to mitigate aero-optical aberrations as a function of viewing angle

**Shaddy Abado,*,† Stanislav Gordeyev, and Eric Jumper**
[a]University of Notre Dame, Institute for Flow Physics and Control, Department of Aerospace and Mechanical Engineering, Notre Dame, Indiana 46556, United States

**Abstract.** A comparison between the spatial and temporal requirements for designing adaptive-optic correction systems for aero-optical turbulence over the pupil of a turret on the side of an airborne platform is presented. These systems are necessary to mitigate the deleterious aero-optic effects on an optical beam and to reopen the field of regard. The derived technique makes use of the two-dimensional proper orthogonal decomposition to characterize the spatial and temporal frequencies of in-flight measured data from the Airborne Aero-Optics Laboratory. For this study, 13 different viewing angles, which represent various flow topologies around the airborne turret, were chosen. The paper concludes with a discussion that points out the usefulness of the derived technique in characterizing the aero-optical disturbances of various aero-optical environments at different viewing angles and different turret configurations.  [DOI: 10.1117/1.OE.53.10.103103]

Keywords: aero-optics; adaptive-optics; proper orthogonal decomposition; airborne aero-optics laboratory; wavefront sensor; deformable mirror; hemisphere-on-cylinder turret; flat windowed turret.

Paper 140941 received Jun. 11, 2014; revised manuscript received Aug. 26, 2014; accepted for publication Sep. 4, 2014; published online Oct. 7, 2014.

## 1 Introduction

Aero-optics[1,2] refers to the aberrations imposed on an otherwise-planar wavefront of a laser propagated through near-field turbulence in flows over and around a turret on an airborne laser platform. The magnitude of these aberrations can be quite large depending on the flight altitude and Mach number as well as the pointing direction, which is commonly described with the azimuthal (AZ) and elevation (EL) angles of the outgoing beam, referenced to the angle of the flight relative wind (i.e., Az 0.0 deg, El 0.0 deg being directly into the flight direction).[3] The magnitude of these aberrations can be sufficiently large to greatly reduce the system's useful field of regard. Adaptive-optics,[4] which attempts to place a conjugate wavefront on the beam before it propagates through the turbulence, could theoretically reopen the field of regard; however, both the spatial and temporal frequencies contained in the aberrations make conventional adaptive-optic approaches minimally effective and often cause worse aberrations than are present with no "correction."[5]

Until recently, the only available experimental wavefront measurements of aero-optical disturbances around airborne turrets have come from wind-tunnel experiments[6] and numerical simulations,[7] and no flight-tests were available to verify if the aero-optical disturbances are also present to the same degree in flight conditions. To address this need, an Airborne Aero-Optical Laboratory (AAOL) was designed, and a series of experiments were carried out.[8]

As shown in Ref. 9, the flow topology characteristics around the airborne turret and consequently the adaptive-optics system requirement are wavefront-dependent. Therefore, to fully characterize the adaptive-optics system's requirement for an airborne turret, an analysis of the system's requirements for different viewing angles is necessary.

An initial analysis of the AAOL dataset was presented in our previous paper,[10] where a four beam Malley probe technique was derived and applied to two wavefront datasets to determine the two-dimensional (2-D) velocity distributions across the beam's aperture. The research described in this paper expands this initial research by exploring new analysis techniques for analyzing and manipulating the in-flight measured wavefronts. This technique begins with applying the 2-D proper orthogonal decomposition (POD)[11] to the in-flight measured datasets to characterize the nature of the aberration field around the airborne turret due to flow structures convecting over the aperture. The analysis techniques presented in this paper for determining the basic character of the aberrations were also shown to be helpful in determining the spatial and temporal requirements of deformable mirrors in an adaptive-optics correction system at various viewing angles. The datasets analyzed in this paper were acquired to capture the aero-optical aberrations around a flat-windowed, hemisphere-on-cylinder turret. In the presence or absence of flow control, this sort of information should be helpful in developing a set of simplified benchmarks and guidelines for determining the minimum requirements an adaptive-optics system needs to meet to effectively mitigate the deleterious aero-optic effects on the beam.

The paper is structured as follows: A description of the in-flight measured dataset and the scaling laws is presented in Sec. 2. An analysis of the nondimensional, time-averaged, root-mean-square optical path difference, $\overline{\mathrm{OPD}}_{\mathrm{rms}}^{\mathrm{ND}}$, as a function of viewing angle is presented in Sec. 3. An analysis of the aperture-averaged subaperture power spectral density as

*Address all correspondence to: Shaddy Abado, E-mail: sabado@alumni.nd.edu

†This work was performed while the author was a graduate student at the Department of Aerospace and Mechanical Engineering, University of Notre Dame.

a function of viewing angle is presented in Sec. 4. A summary of the POD application to the AAOL is presented in Sec. 5. In Sec. 6, the POD's energies as a function of the viewing angle are presented. A brief description of the proposed methodology to determine the spatial and temporal frequencies for aero-optics correction based on the POD analysis is presented in Sec. 7. The spatial and temporal requirements of the adaptive-optics system as a function of viewing angle are presented in Sec. 8. Finally, the paper concludes with a brief discussion of the results.

## 2 Viewing Angle, Modified Elevation Angle, and Application Flight Scenario

As mentioned in Sec. 1, the direction of the outgoing laser beam emerging from the optical-window relative to the incoming freestream flow is typically described using the AZ, $\alpha_{\mathrm{Az}}$, and EL, $\alpha_{\mathrm{El}}$, angles coordinate system. However, from a flow-physics point of view, it is more convenient to introduce a viewing angle, $\alpha_{\mathrm{Vi}}$, and a modified EL angle, $\alpha^{m}_{\mathrm{El}}$, coordinate system to describe the beam direction. The viewing angle is defined as the angle between the flow direction and beam direction vectors, whereas the modified EL angle is defined as the angle between the junction plane joining the hemisphere to the cylinder and the plane formed by the flow direction and the beam direction vectors.[3] These two angles are calculated from the AZ and the EL angles through the following two equations

$$\cos(\alpha_{\mathrm{Vi}}) = \cos(\alpha_{\mathrm{El}}) \cdot \cos(\alpha_{\mathrm{Az}}), \tag{1}$$

$$\tan(\alpha^{m}_{\mathrm{El}}) = \frac{\tan(\alpha_{\mathrm{El}})}{\sin(\alpha_{\mathrm{Az}})}. \tag{2}$$

If the AZ angle is 0 deg, then the viewing angle coincides with the EL angle ($\alpha_{\mathrm{Vi}} = \alpha_{\mathrm{El}}$), and if the AZ angle is 180 deg, then $\alpha_{\mathrm{Vi}} = 180\ \mathrm{deg} - \alpha_{\mathrm{El}}$.

It is common to present wavefront results in nondimensional quantities for scaling to any relevant flight conditions and turret configurations different in dimensions than those experienced during the in-flight data collection. As such, the optical path difference (OPD),[4] spatial frequency, and temporal frequency presented in this paper were first nondimensionalized similar to the scaling laws proposed in Refs. 9 and 12. For the purpose of this study, we chose to re-scale the AAOL experimental data to an application flight at 25 kft, Mach of 0.5, turret diameter of $D_t = 1$ m, aperture diameter of $D_{\mathrm{Ap}} = D_t/3 = 1/3$ m, and 1-$\mu$m wavelength laser. The wavefront data was collected with a high-speed Shack–Hartmann[4] wavefront sensor framing at 20 kHz.

## 3 Nondimensional, Time-Averaged, Root-Mean-Square OPD as a Function of Viewing Angle

The nondimensional, time-averaged, root-mean-square OPD, $\overline{\mathrm{OPD}^{\mathrm{ND}}_{\mathrm{rms}}}$, of a large range of viewing angles can be calculated for better understand the level of the aero-optical disturbances around the turret. Figure 1 shows a plot of the $\overline{\mathrm{OPD}^{\mathrm{ND}}_{\mathrm{rms}}}$ values for 13 different viewing angles. These 13 viewing angles represent various flow topologies around the airborne turret and were measured throughout the AAOL project.[8] Tip and tilt aberrations were removed from all viewing angles datasets.

The $\overline{\mathrm{OPD}^{\mathrm{ND}}_{\mathrm{rms}}}$ values in Fig. 1 agree with the flow-field topological characteristics which were presented in Ref. 9. These main characteristics are presented in the plot and summarized here. For small forward-looking viewing angles, the values are small; therefore, the optical aberrations are negligible. However, as the viewing angle increases, the level of optical aberration also increases due to a local separation bubble which forms around the aperture. A local peak in the level of optical aberration is achieved approximately at a 93-deg viewing angle. After this local peak, the level of optical distortion decreases. This degradation in the level of optical aberrations contributes to the effects of removing tip/tilt aberrations.[13] For viewing angles larger than 100 deg, the level of optical disturbances increases substantially. For more discussion of the aero-optical distortions as a function of the aperture angle, see Refs. 9 and 14.

Based on Fig. 1, we would expect significant performance degradation for systems which are operating at viewing angles larger than ~80 deg. This performance degradation can be associated to the large flow structures which form

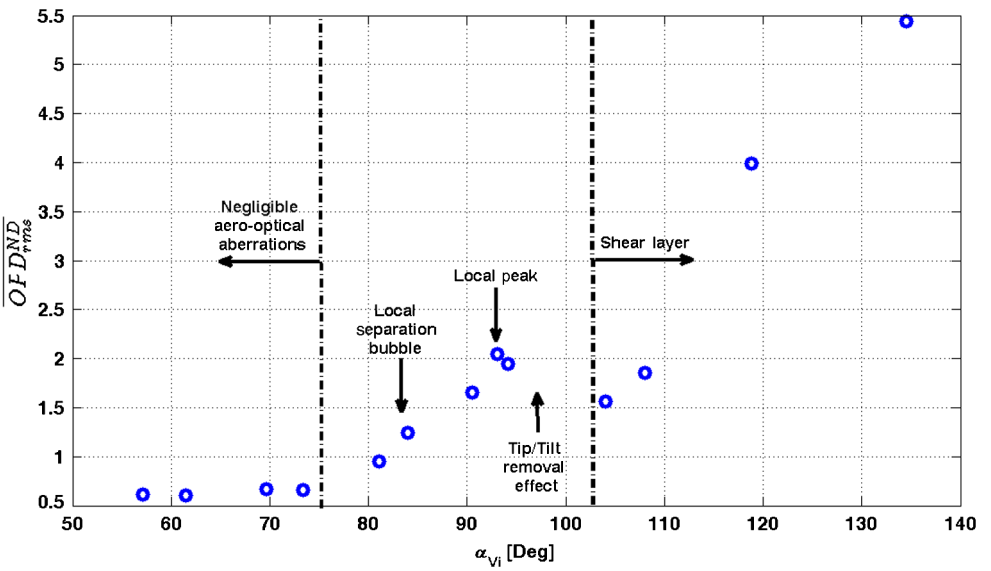


**Fig. 1** $\overline{\mathrm{OPD}^{\mathrm{ND}}_{\mathrm{rms}}}$ as a function of viewing angle (46 deg < $\alpha^{m}_{\mathrm{El}}$ < 79 deg).

at this viewing angle range. The main characteristics of the aero-optical disturbances discussed in this section will be used to explain the major results presented in this paper.

## 4 Power Spectral Density as a Function of Viewing Angle

The temporal spectral analysis can be used to characterize the flow-field's topology at various viewing angles. In this section, the aperture-averaged subaperture power spectral density (PSD), as it was defined in Ref. 10, is calculated for various viewing angles to validate the flow-field's topology characteristics which were presented in Sec. 3.

Figure 2 shows PSD plots of different viewing angles. The PSD curves were vertically shifted to reflect the viewing angle of each in-flight measured dataset. The spectrum curve can be loosely interpreted in terms of the energy associated with eddies of various sizes.[15] For small forward-looking viewing angles, the spectra are quite uniform and are not dominated by specific features. This indicates that the aero-optical disturbances at these forward-looking viewing angles are not affected by higher-order aero-optical aberrations and are characterized by small size eddies. These small eddies contribute to the large frequency components of the spectrum. As the viewing angle increases, a broadband hump appears in the spectra at an ~104- deg viewing angle. This trend is expected if the aero-optical disturbance is produced by coherent structures, which are associated with the shear layer due to a separated flow.[16] These large coherent structures contribute to the low frequency components of the spectrum. As the viewing angle increases, the broadband hump's magnitude increases and it can be seen shifting to lower frequencies in the spectra.

## 5 Application of POD to the AAOL

The POD is a linear procedure which decomposes a set of data signals (snapshots) which are varying in both space and time into the optimal linear basis (modes) possible. Hence, it can find a new set of dimensions that better capture the variability of the data. The POD was developed by several people and can be traced back to Karhunen[17] and Loève.[18] A comprehensive discussion of the POD technique can be found in Ref. 11. In the context of turbulence, the POD was introduced by Lumley.[19] The useful aspect about using POD is that it separates the modal structures by their contribution to the overall aero-optical "energy" or $\mathrm{OPD}^2_{\mathrm{rms}}$, providing a quantitative measure of the aberrations due to that mode.[12] The POD analysis splits the spatiotemporal field into a series of statistically-independent, stationary, spatial patterns (spatial modes), $\varphi_n(x,y)$, and corresponding time-dependent coefficients (temporal coefficients), $a_n(t)$. This split simplifies the interpretation of the dominant wavefront structures and their characteristics. Based on this, the temporal coefficients and the spatial modes can be used to reconstruct the original in-flight measured wavefronts-field, $\mathrm{OPD}^{\mathrm{Org}}_n(t,x,y)$. The reconstructed wavefronts-field can be expressed as

$$\mathrm{OPD}^{\mathrm{Re}\,c}_n(t,x,y)=\sum_{i=1}^{n} a_i(t)\cdot\varphi_i(x,y), \tag{3}$$

where $n$ is the number of modes used to reconstruct the wavefronts' dataset.

The residual error of comparing the reconstructed wavefronts' dataset and the original in-flight measured wavefronts' dataset can be defined as

$$\mathrm{OPD}^{\mathrm{Error}}_n(t,x,y)=\mathrm{OPD}^{\mathrm{Org}}(t,x,y)-\mathrm{OPD}^{\mathrm{Re}\,c}_n(t,x,y). \tag{4}$$

An initial application of the POD to the AAOL data was presented in Ref. 10, where it was shown that the overall amplitude of the temporal coefficients, and hence their relative contribution to the total "energy," decreases as the mode number increases. There would be no reason to expect *a priori* that the temporal coefficients would have the same frequency content as the original dataset. However, both the in-flight measured OPD's dataset, $\mathrm{OPD}^{\mathrm{Org}}(t,x,y)$, and the temporal coefficients are driven by the same mechanism within the flow, namely the largest, coherent structures. Therefore, the wavefronts' time evolution characterization can be identified in the temporal frequency spectra of the POD temporal coefficients.

Let $\Psi_n(f_t)$ be the temporal PSD of POD temporal coefficient $a_n(t)$. Then, the PSDs of the sum of temporal coefficients starting from the first mode until mode $n$, $\Psi_{\sum_{i=1}^{n} a_i(t)}$, are shown in Fig. 3 for $\alpha_{\mathrm{Vi}} \sim 134$ deg and $n = 1, 2, 3, 4, 10$

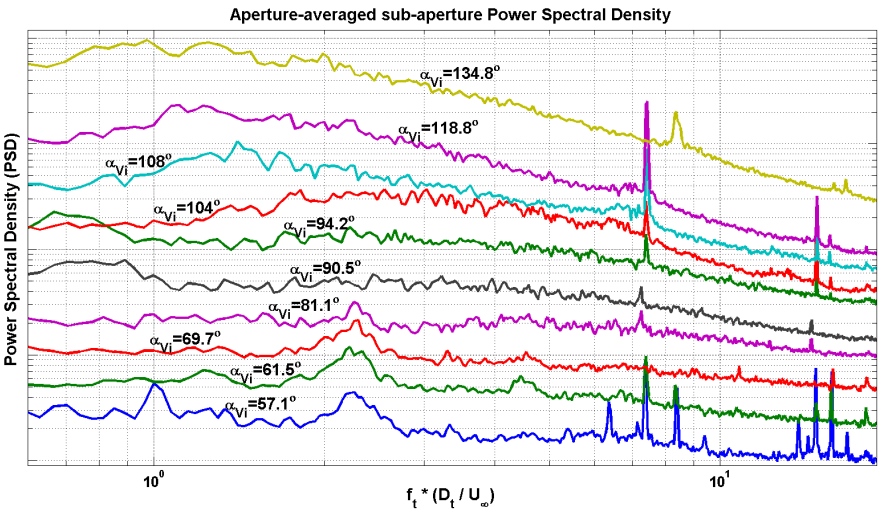


**Fig. 2** Aperture-averaged subaperture power spectral density as a function of viewing angle.

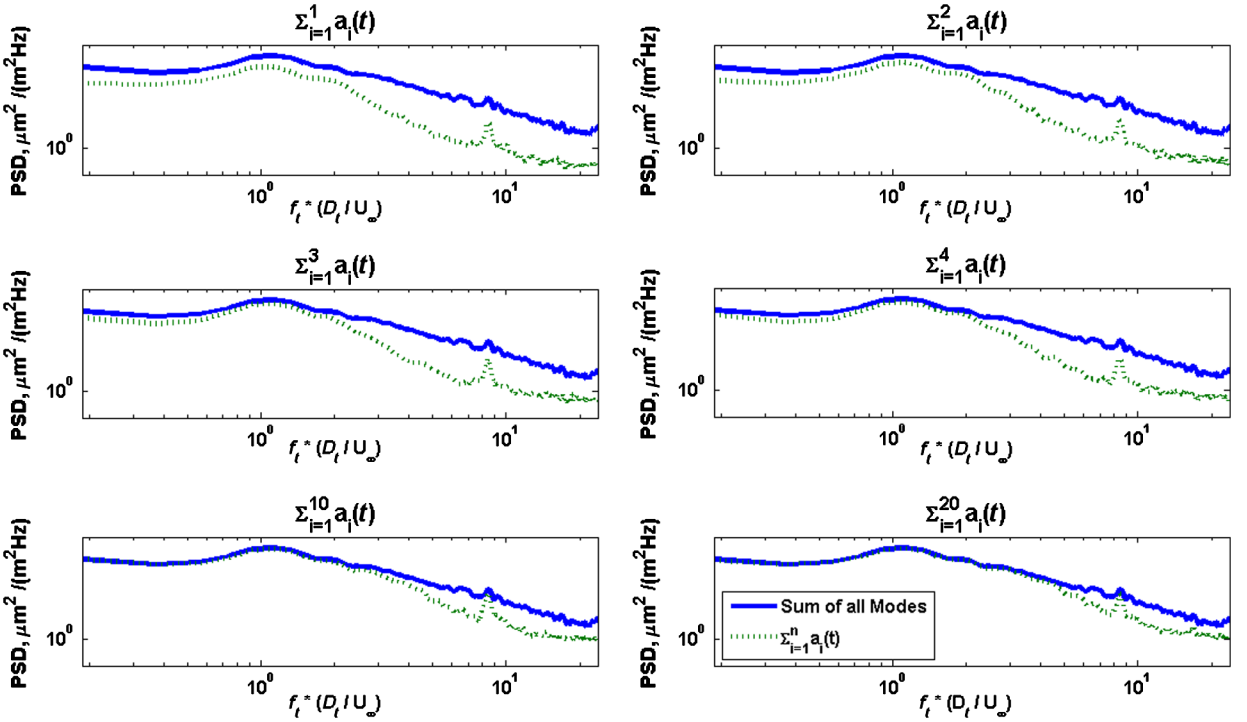


**Fig. 3** Power spectral density of $\Psi_{\sum_{i=1}^{n} a_i(t)}$ $\alpha_{Vi} \sim 134$ deg and $n = 1, 2, 3, 4, 10, 20$.

and 20. Each PSD is compared with the PSD of the sum of all temporal coefficients, $\Psi_{\sum_{i=1}^{N_{total}} a_i(t)}$. As expected, it can be clearly noticed that as more temporal coefficients are added, the more $\Psi_{\sum_{i=1}^{n} a_i(t)}$ resembles $\Psi_{\sum_{i=1}^{N_{total}} a_i(t)}$. In addition, the low-order temporal coefficients reflect the low temporal frequency content of the wavefronts' disturbances, whereas the high-order temporal coefficients reflect the high temporal frequency content of the wavefronts' disturbances. Furthermore, the sum of the first four temporal coefficients is sufficient to resolve the broadband hump, which indicates the presence of large-scale coherent structures due to the presence of a shear layer.[10,16] This shear layer develops from the separation point on the turret and dominates the separated flow at large aft-looking viewing angles, similar to the angle presented here.

It was shown in Ref. 10 that the first four spatial modes reflect the presence of large-scale coherent structures. Similarly, we can conclude, based on Fig. 2, that it takes four temporal coefficients to resolve the broadband hump in terms of energy. In addition, the convective nature of these four modes, which was presented in our previous paper,[10] is consistent with the local phase convective velocity mapping which also was presented in the same paper and was performed over the same broadband hump frequency range.

## 6 POD "Energy" as a Function of Viewing Angle

The POD can be used to separate the aero-optical disturbance into modal structures ordered according to their contribution to the overall aero-optical "energy" or $OPD_{rms}^2$, providing the quantitative measure of the aberrations due to that mode.[12] In this section, the POD technique is applied to various viewing angles to analyze and compare between their modal "energy" content.

The number of modes required to resolve 50% (~3 dB), 75% (~12 dB), and 90% (~0.45 dB) of the disturbance "energy" as a function of viewing angle is shown in Fig. 4(b). Due to the slightly different test configuration of each viewing angle's dataset, the number of subapertures analyzed varied between the tests; therefore, the total number of POD modes at each dataset was also different. The percentage of the number of modes required to resolve these percentages of "energy" is shown in Fig. 4(a).

As expected, the percentage of the number of modes required to resolve a certain percentage of "energy" increases as the required percentage of "energy" increases; however; this increase is not linear. For example, the increase in the additional percentage of modes which is necessary to increase the required percentage of resolved "energy" from 75% to 90% is larger than the increase in the additional percentage of modes which is necessary to increase the required percentage of resolved "energy" from 50% to 75%. This observation indicates that for almost all viewing angles, the majority of the "energy" is in the content of the small order modes; therefore, a small increase in the number of modes significantly increases the resolved "energy."

It can be also seen that the shapes of the curves in Fig. 4 are correlated with the shape of the curve in Fig. 1. For example, for forward-looking viewing angles, the percentage of the number of modes increases as the viewing angle increases. The percentage of the number of modes reaches a local maximum value at the same viewing angle range where a local separation bubble starts forming at approximately $\alpha_{Vi} = 80$ deg. This increase in the percentage of number of modes for the forward-looking viewing angles can be related to the fact that, for these viewing angles, the flow-field creates pseudosteady-lensing aberrations, such as defocus and coma, which are left after removing the mean aberrations. Also, as the viewing angle increases,

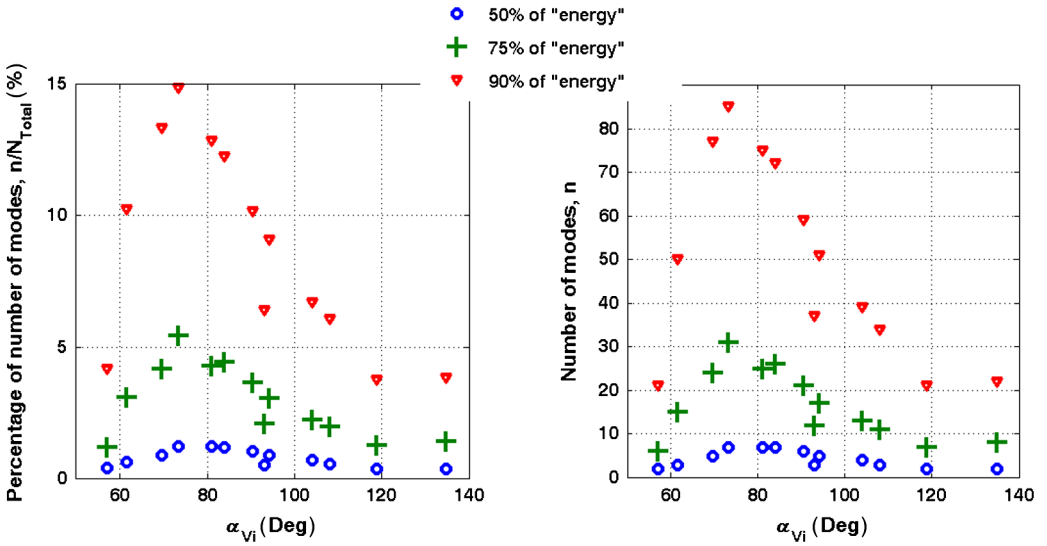


**Fig. 4** Number of proper orthogonal decomposition modes required to resolve 50%, 75%, and 90% of the "energy:" (a) percentage of number of modes versus viewing angle; (b) number of modes versus viewing angle.

the complexity of these aberrations also increases;[9] therefore, a large number of POD modes are required to resolve these structures.

As the local separation bubble increases beyond $\alpha_{Vi} \sim 80$ deg, the coherent structures over the beam's aperture become larger and more dominant; therefore, less POD modes are required to resolve these structures, and hence the decrease in the curves' values in Fig. 4.

The required percentage of the "energy" curve in Fig. 4 reaches a minimum at approximately $\alpha_{Vi} \sim 90$ deg, which is the same viewing angle where the $\overline{OPD}_{rms}^{ND}$ curve in Fig. 1 reaches its local peak value. Afterward, the curves in Fig. 4 exhibit an increase in the percentage of the number of modes. This increase can be attributed to the effects of removing tip/tilt aberrations, where, because of the removal of large structures by $Z$-tilt correction, smaller coherent structures are left to be resolved.[13] Resolving these smaller coherent structures requires more POD modes, and hence the increase in the curves' values.

It was shown in Fig. 4 that for backward-looking viewing angles, the level of optical disturbance increases substantially. This increase is due to large, energetic, coherent structures which dominate the flow-field. The POD analysis resolves the majority of these coherent structures in a few POD modes; therefore, fewer modes are required to resolve a given percentage of "energy," and the curves' values in Fig. 4 decrease as the viewing angle increases.

Based on all of the conclusions presented above, only a few modes relative to the total number of possible POD modes are required to resolve and compensate for the majority of the spatial and temporal contents of the aero-optical disturbances. This observation is especially true for the backward-looking viewing angles, which impose the most constraining aero-optical disturbances.

## 7 Approach to Spatial and Temporal Frequencies for Aero-Optics Correction Based on the POD

The results of Sec. 6 indicate that when correcting for aero-optical disturbances, the primary correction should account for the low-order modes as they contain the most dominant and energetic spatial and temporal features of the flow-field. It can also be shown that the efficiency of the adaptive-optics correction depends upon various parameters,[4] such as the type of spatial correction applied, the resolution of the spatial correction, and the correction-update rate. The spatial and temporal requirements to mitigate aero-optical aberrations using adaptive-optics system, and the influence of the systems' parameters on its performance, will be analyzed and discussed further in this section.

### 7.1 *Spatial Requirements*

The spatial resolution of the adaptive-optics correction is limited by the deformable mirror, which is used to imprint the conjugate wavefront phase onto the optical beam. In our previous paper,[10] it was shown that it is possible to characterize the spatial extent of the coherent structures and to obtain the specific spatial requirements in the flow and cross-flow directions by calculating the correlation length of each spatial POD mode. For the purpose of our analysis, the correlation length was defined as the location of the auto-correlation function's first minimum.[20,21] Denoting the correlation length of the spatial POD mode $n$ as C.L.$^n$, then its spatial frequency, $f_s^n$, can be defined as

$$f_s^n = 1/\text{C.L.}^n, \tag{5}$$

and the number of periods of aberrations per aperture, 1/Aperture, can be defined as

$$1/\text{Aperture} = D_{Ap} \cdot f_s^n. \tag{6}$$

Once the coherent structures have been identified based on the POD technique and characterized by their correlation lengths, it is possible to determine the spatial requirements of an adaptive-optics system for aero-optical disturbances. To analyze the spatial requirements of the system, it is necessary to define the number of required actuators per aperture parameter, Actuators/Aperture, as

$$N^{n}_{\mathrm{Re}\,q} = 2 \cdot D_{\mathrm{Ap}} \cdot f^{n}_{s}. \quad (7)$$

This parameter is the minimum number of deformable mirror actuators per turret's aperture which are required to compensate for the coherent structure of the POD mode $n$. Based on Eq. (7), the number of required actuators per aperture can be calculated to determine the spatial requirements as a function of a mode number.

It was shown in Sec. 5 that it is possible to calculate the time-averaged, root-mean-squares, residual error of the reconstructed wavefronts' dataset, $\overline{\mathrm{OPD}^{\mathrm{Error}}_{\mathrm{rms}}}$, as a function of mode number $n$, where the reconstruction residual was defined in Eq. (4). Based on this, it is possible to relate the number of actuators per aperture of the deformable mirror to a correction residual error value, where each mode number is replaced with its associate $\overline{\mathrm{OPD}^{\mathrm{Error}}_{\mathrm{rms}}}$ value. Knowing the time-averaged, root-mean-squares, residual errors, it is possible to calculate the Strehl ratio[22] based on the large aperture approximation.[4,22,23]

### 7.2 *Temporal Requirements*

After analyzing the spatial requirements that the aero-optical disturbances impose on an adaptive-optics corrective system, the temporal requirements need to be analyzed. The spatial analysis, which was discussed above, assumed no time latency in applying the aero-optical correction. In this section, a perfect spatial adaptive-optic correction is assumed to investigate the effects of time latency, temporal sampling frequency, and loop gain on the corrective adaptive-optics system's performance.

As was discussed in Sec. 5, the temporal coefficients of the POD analysis contain the temporal characteristics of the aero-optical disturbances. Based on these temporal coefficients, it is possible to simulate the response of a close-loop, conventional adaptive-optics system to disturbances by applying a filter in the frequency domain. The response of the close-loop control system to disturbances in the frequency domain can be considered to be a function of $F_S$, the discrete-time sampling frequency, $\beta$, the loop gain, and $\Delta t$, the net latency of the control system. If each temporal coefficient contains different spectral features, then applying the filter to each temporal coefficient will reject different spectral content from each mode. A summary of this correction procedure is available in Ref. 12.

It is possible to perform various simulations to demonstrate the effects of varying the three closed-loop system's parameters ($F_S$, $\beta$, and $\Delta t$) on the adaptive-optics system performance. Figure 5 presents a simulation to assess the relationship between the Strehl ratio and the loop gain for four values of 0.25, 0.5, 0.75, and 1 frame latencies. For each value of frame latency, four temporal sampling frequencies were tested. Here, an application flight scenario at $\alpha_{\mathrm{Vi}} \sim 134$ deg is assumed. It can be concluded from Fig. 5 that for a constant time latency value, the system's performance improves as the temporal sampling frequency increases. It can also be concluded that for a constant temporal sampling frequency value, the system's performance improves as the time latency decreases.

## 8 Spatial and Temporal Requirements as a Function of Viewing Angle

After analyzing the datasets of the various viewing angles using the PSD and POD analyses and linking the POD parameters (temporal coefficients and spatial modes) to the adaptive-optics system required specifications, the POD technique will be used to determine the spatial and temporal requirements of the adaptive-optics system as a function of the viewing angle. For the analysis in this section, we attempt to investigate the system's requirements at the most demanding viewing angles; therefore, viewing angles smaller than 81 deg will not be considered in the analysis.

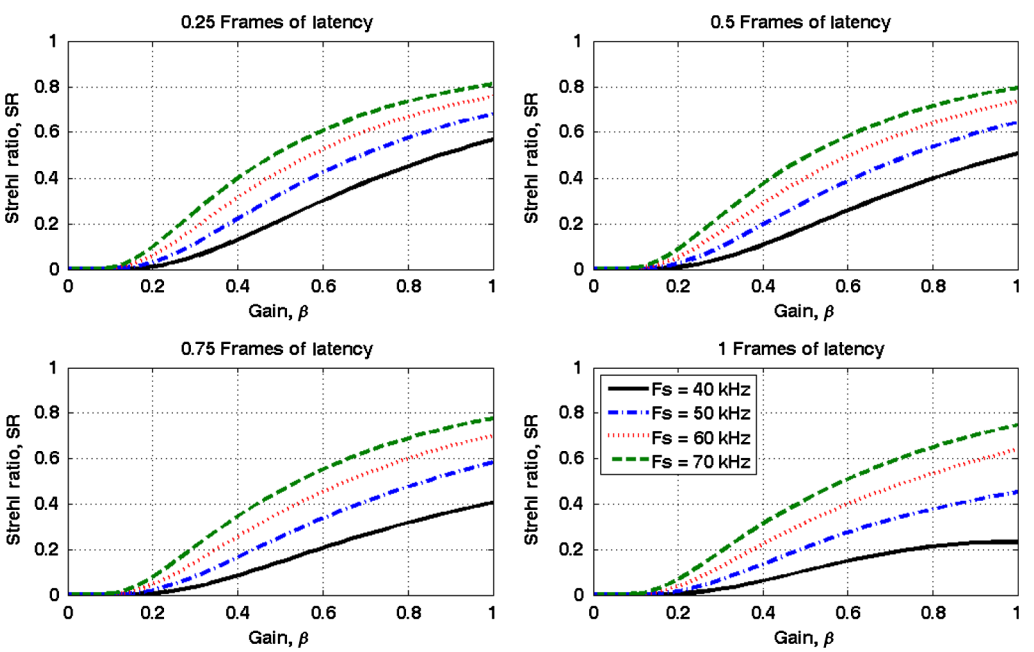


**Fig. 5** Strehl ratio versus loop gain for 0.25, 0.5, 0.75, and 1 frames of latency for an application flight scenario at $\alpha_{\mathrm{Vi}} \sim 134$ deg.

### 8.1 *Spatial Requirements*

The number of actuators per aperture required to achieve Strehl ratio[22] values of 0.7 (~1.5 dB), 0.8 (~0.96 dB), and 0.9 (~0.45 dB) as a function of the viewing angle are shown in Fig. 6 for the streamwise and spanwise directions in the turret frame of reference. This number of actuators per aperture was calculated based on the approach derived in Sec. 7. The values in the plots are scaled to an application flight scenario as it was defined in Sec. 2. As expected, for a constant viewing angle, the number of required actuators per aperture increases as the Strehl ratio increases. This observation is true for both flow directions. In addition, for a constant Strehl ratio and a constant viewing angle, the number of required actuators per aperture is larger for the streamwise direction than for the spanwise direction. These two observations are consistent with the results reported in Ref. 10.

The shape of the curves in Fig. 6 can be related to the shape of the curve in Fig. 1. Based on Fig. 1, it was concluded that the level of aero-optical disturbances increases as the local separation bubble develops. In Fig. 6, this increase in the level of aero-optical disturbances corresponds to an increase in the number of required actuators per aperture due to the higher spatial resolution required to resolve the aero-optical disturbances; however, at a certain viewing angle, the spatial system requirements decrease. This decrease is due to the removal of tip/tilt aberrations which compensate for the dominant aero-optical disturbances; therefore, we are left to correct for less demanding aero-optical disturbances. For backward-looking viewing angles, the sharp increase in the level of aero-optical disturbances due to the shear layer corresponds to an increase in the number of required actuators per aperture. It is interesting to note here that the number of required actuators per aperture for the backward-looking viewing angles is not much larger than the number of required actuators per aperture for the separation bubble viewing angle range. This observation indicates that while the sources of aero-optical disturbances are different, the spatial requirements of both flow regimes are very similar.

Plots of the Strehl ratio as a function of the viewing angle for 10, 15, and 20 actuators per aperture are shown in Fig. 7 for the streamwise and spanwise directions. The values in the plots are scaled to an application flight scenario. It is interesting to note that for almost all viewing angles, and especially for the backward-looking viewing angles, increasing the number of actuators per aperture from 10 to 15 improves the Strehl ratio value more significantly than increasing the number of actuators per aperture from 15 to 20. This observation indicates that once the dominant, low spatial frequency, coherent structures are corrected then the uncorrected, high spatial frequency, coherent structures impose less demanding aero-optical disturbances. In addition, it can be noticed that for backward-looking viewing angles, a deformable mirror with at least 20 actuators per aperture is required to achieve a decent correction.

### 8.2 *Temporal Requirements*

It was concluded in Ref. 5 that the dominant system requirements are set by the temporal frequencies of the aero-optical disturbance. In this section, we attempt to re-verify this conclusion and compare the system's temporal requirements for different viewing angles.

For this subsection, we chose to analyze an adaptive-optics system with zero time latency and 0.5 loop gain. Plots of the Strehl ratio as a function of temporal sampling frequency for different viewing angles are shown in Fig. 8. Based on this figure, it can be concluded that for a constant temporal sampling frequency, the Strehl ratio decreases as the viewing angle increases, excluding the viewing angles' range of 90 to 94 deg, where a local peak in the level of optical aberration is achieved due to the effects of removing tip/tilt aberrations.[13] Similar to the spatial analysis figures, the order of the curves in Fig. 8 can be related to the level of the aero-optical disturbances' curve in Fig. 1. For example, we can notice that for forward-looking viewing angles (the upper four curves), a Strehl ratio larger than 0.8 can be achieved with relatively low temporal sampling frequencies. These temporal requirements are related to the low level of aero-optical disturbances at forward-looking viewing angles, where the flow-field is dominated by a thin

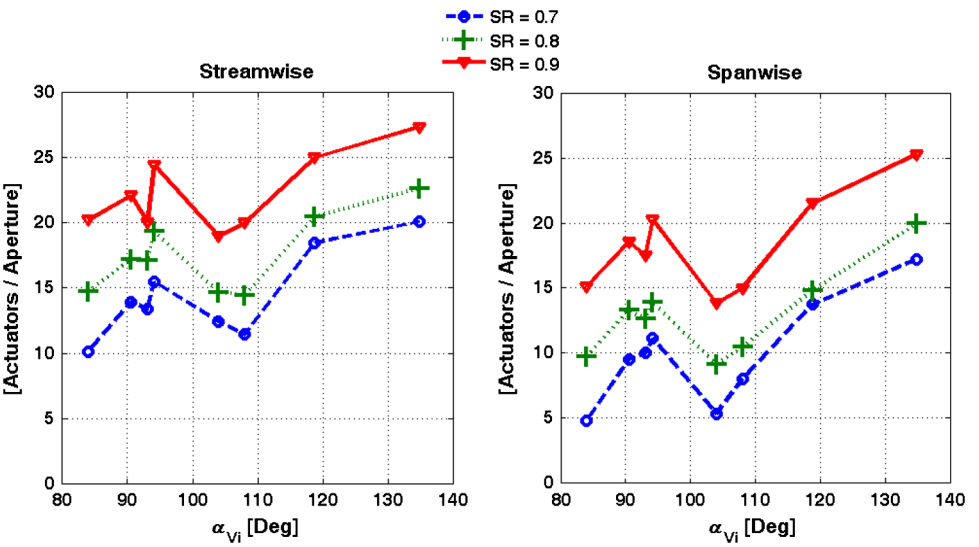


**Fig. 6** Number of required actuators per aperture as a function of viewing angle for Strehl ratios of 0.7, 0.8, and 0.9 (application flight scenario).

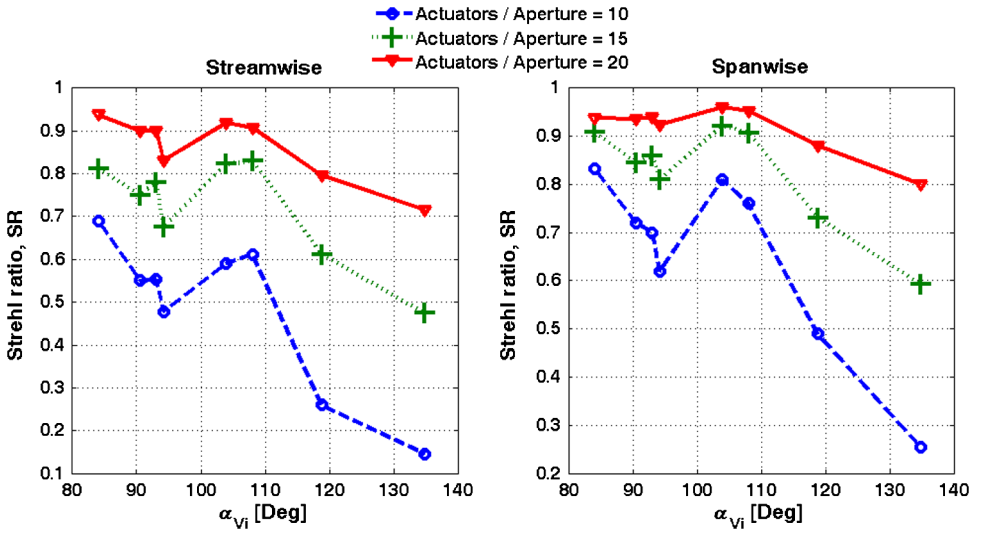


**Fig. 7** Strehl ratio as a function of viewing angle for number of required actuators per aperture of 10, 15, and 20 (application flight scenario).

attached boundary layer due to the favorable pressure gradient.

As the viewing angle increases, the Strehl ratio for a constant temporal sampling frequency decreases, reaching a minimum at a ~94-deg viewing angle. This decrease in the system's performance is related to the increase in the level of aero-optical disturbances due to the local separation bubble. Based on Fig. 2, we concluded that the development of the local separation bubble across the beam's aperture is associated with an increase in the temporal frequency content. This conclusion explains the significant increase in the system's temporal requirement at this viewing angle's range. As the viewing angle increases past this range, the system's performance exhibits an improvement for a small range of viewing angles due to the tip/tilt correction. However, for backward-looking viewing angles larger than $\alpha_{Vi} \sim 110$ deg, the system's performance decreases significantly (the lower two curves). Therefore, this viewing angle's range imposes the most demanding system requirements.

To better evaluate the temporal performance of an adaptive-optics system as a function of the viewing angle, it is possible to perform an analysis based on Fig. 8 where the temporal sampling frequency is set to a constant value and the Strehl ratio at this temporal sampling frequency value is determined for each viewing angle. Figure 9 presents the Strehl ratio as a function of the viewing angle for 10, 50, and 100-kHz temporal sampling frequencies. We can notice that each of the curves in the figure is almost identical to the conjugate image of the level of aero-optical disturbances

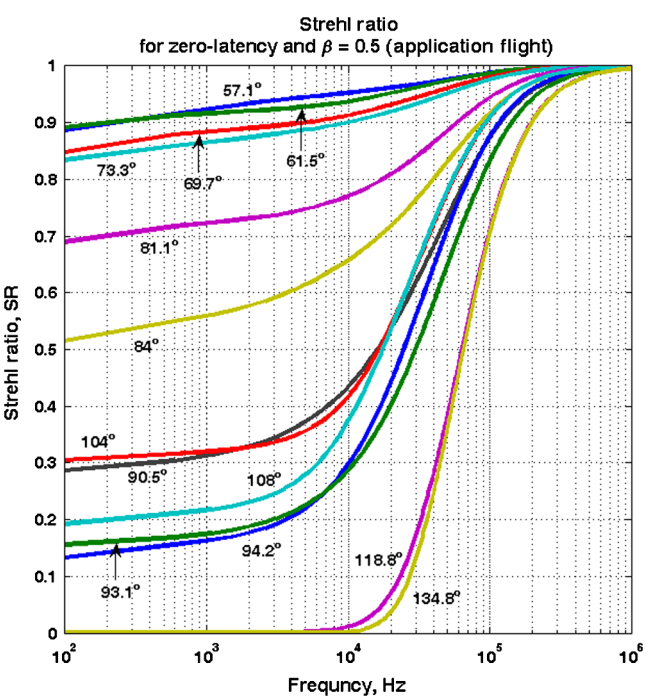


**Fig. 8** Strehl ratio as a function of temporal sampling frequency for different viewing angles (application flight scenario).

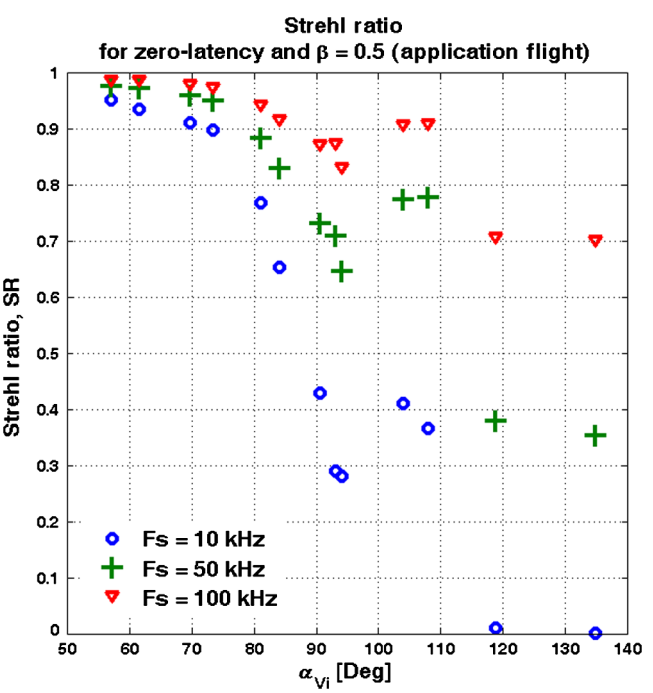


**Fig. 9** Strehl ratio as a function of viewing angle for temporal sampling frequencies of: 10, 50, and 100 kHz (application flight scenario).

curve in Fig. 1. As expected from Fig. 8, for forward-looking viewing angles, the increase in sampling frequency has a negligible effect on the system's performance. However, as the viewing angle increases, the increase in the temporal sampling frequency notably improves the system's performance. This observation especially holds for backward-looking viewing angles.

### 8.3 *Combining the Spatial and Temporal Requirements as a Function of Viewing Angle*

In the previous two subsections, we showed that the system's spatial and temporal requirements reflect the level of aero-optical disturbances. In addition, we showed that the dominant system's requirements are set by the aero-optical disturbances' temporal frequencies, especially for backward-looking viewing angles. In this subsection, we attempt to combine the spatial and temporal requirements and show the dependency of the total Strehl ratio values on the viewing angle. Using the large-aperture approximation,[3] the total Strehl ratio, $SR_{Total}$, can be calculated as

$$SR_{Total} = SR_{Spatial} \cdot SR_{Temporal}, \tag{8}$$

where $SR_{Spatial}$ is the Strehl ratio based on the spatial residual variance, and $SR_{Temporal}$ is the Strehl ratio based on the temporal residual variance. Assuming a zero time latency and 0.5 loop gain, the total Strehl ratio as a function of viewing angle for 10, 50, and 100-kHz temporal sampling frequencies were calculated for 15 actuators per aperture, Fig. 10(a), and 20 actuators per aperture, Fig. 10(b).

As expected from the spatial and temporal system requirements, for a constant viewing angle, the total Strehl ratio increases as the number of actuators per aperture, or the temporal sampling frequency, increases. A better look at Fig. 10 may reveal that the improvement in the total Strehl ratio value due to the increase in the temporal sampling frequency

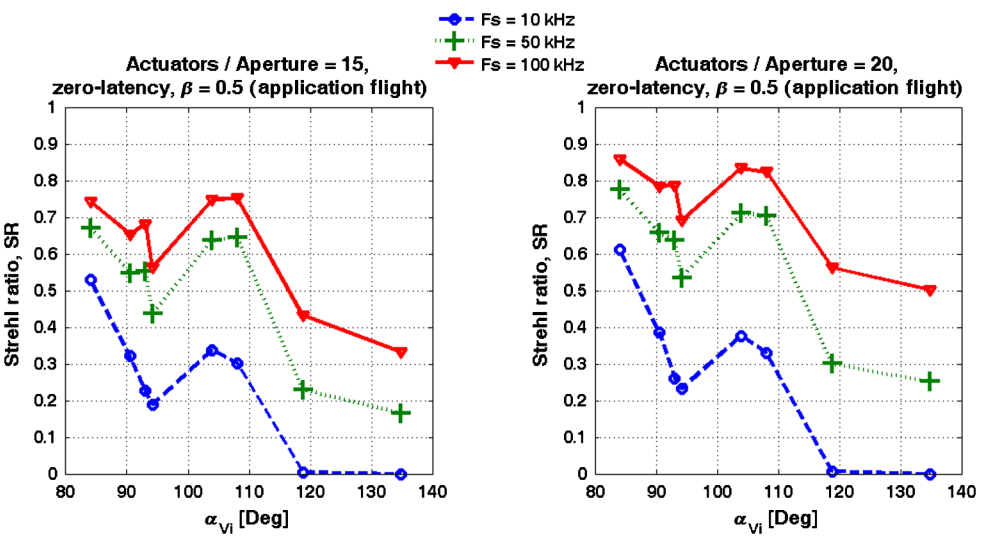


**Fig. 10** Total Strehl ratio as a function of viewing angle for 10, 50, and 100-kHz temporal sampling frequencies. (a) 15 actuators per aperture; (b) 20 actuators per aperture (application flight scenario).

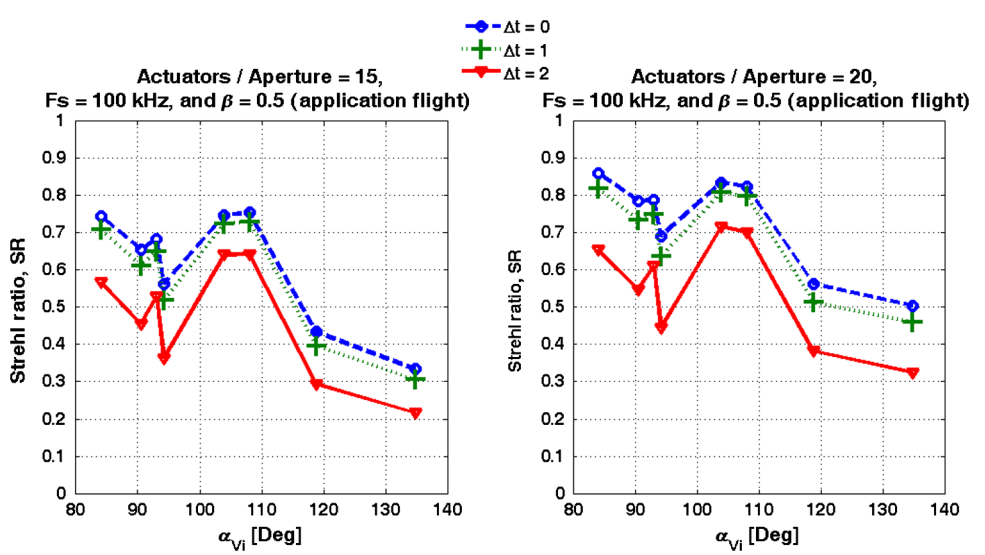


**Fig. 11** Total Strehl ratio as a function of viewing angle for 0, 1, and 2 frames of latency. (a) 15 actuators per aperture; (b) 20 actuators per aperture (application flight scenario).

is more significant for backward-looking viewing angles than it is for forward-looking viewing angles.

It should be noted that the results which were presented in Fig. 10 are for a theoretical case of zero-time latency. For a real system, we can expect the system to exhibit time latency; therefore, the time latency should be included in the analysis. Assuming a 0.5 loop gain and 100-kHz temporal sampling frequency, the total Strehl ratio as a function of viewing angle for 0, 1, and 2 frames of latency were calculated for 15 actuators per aperture, Fig. 11(a), and 20 actuators per aperture, Fig. 11(b). As expected, an increase in the time latency decreases the total Strehl ratio. It is interesting to note that the total Strehl ratio values for a 1 frame of latency are not much smaller than the total Strehl ratio values for a zero frame of latency; however, a greater degradation in the total Strehl ratio value is shown for 2 frames of latency.

## 9 Conclusion

The research reported in this paper involved the application of the 2-D POD to in-flight measured wavefronts from a wavefront senor on board the Airborne Aero-Optics Laboratory (AAOL).

Based on the results of this paper's analysis, it is possible to conclude that for forward-looking viewing angles, the dominant system requirements are set by the spatial resolution of the deformable mirror. Here, this resolution was determined by the number of actuators per aperture. Although forward-looking viewing angles possess high spatial frequency content, they result in a milder system's degradation. However, for backward-looking viewing angles, where the spatial and temporal characteristics of the aberrations are more severe, the system's requirements are much more demanding. For these viewing angles, an improvement in the system's parameters, such as faster temporal sampling frequency or more deformable mirror actuators per aperture, significantly enhances the system performance. It was also shown here that the most dominant of these system's parameters are the temporal ones, where, in order to achieve a decent aero-optical correction, a sampling rate which exceeds 100 kHz, and a decrease in the time latency are required.

The results reported in this paper support previous studies which have shown that the bottleneck limitations on the performance of adaptive-optic systems for aero-optic correction are set by the temporal frequencies.[5] In addition, the results of this study are a continuation of several studies conducted in the last few years to develop alternative approaches of designing adaptive-optic systems to mitigate aero-optical aberrations. Some of these studies include an adaptive-optic correction that is based on aperture filtration,[16] changing the adaptive-optic paradigm from feed-back to feed-forward,[24] and an alternative adaptive-optic system which consists of a feed-forward flow control and a phase-locked loop adaptive-optic control strategy.[25]

The insight provided by the derived methodology in this study has implications for the design of future airborne optical systems. Now that the analysis methodology is clearly at hand, repeating the derived methodology to other turret configurations, such as hemispheric-only turrets, window configurations, such as conformal windows, or flight Mach numbers would be of a great benefit for determining the effect of these design and operational parameters on the aero-optical environment and the system's requirements. In fact, an extensive survey of the aero-optical environment at different viewing angles, for both flat-window and conformal-window turrets at different subsonic and low transonic speeds, was recently presented.[14]

### Acknowledgments

These efforts were funded by the High Energy Laser—Joint Technology Office (HEL-JTO) and administered through the Air Force Office for Scientific Research (AFOSR) under Grant Number FA9550-07-1-0574. The US Government is authorized to reproduce and distribute reprints for governmental purposes notwithstanding any copyright notation thereon.

### References

1. E. J. Jumper and E. J. Fitzgerald, "Recent advances in aero-optics," *Prog. Aerospace Sci.* **37**(3), 299–339 (2001).
2. M. Wang, A. Mani, and S. Gordeyev, "Physics and computation of aero-optics," *Ann. Rev. Fluid Mech.* **44**, 299–321 (2012).
3. C. Porter et al., "Flight measurements of the aero-optical environment around a flat-windowed turret," *AIAA J.* **51**(6), 1394–1403 (2013).
4. R. K. Tyson, *Principles of Adaptive Optics*, 2nd ed., Academic Press, Boston (1998).
5. A. M. Nightingale, S. Gordeyev, and E. J. Jumper, "Optical characterization of a simulated weakly compressible shear layer: unforced and forced," *AIAA J.* **47**(10), 2298–2305 (2009).
6. S. Gordeyev et al., "Aero-optical environment around a cylindrical turret with a flat window," *AIAA J.* **49**(2), 308–315 (2011).
7. K. Wang and M. Wang, "Numerical simulation of aero-optical distortions by flow over a cylindrical turret," in *40th AIAA Plasmadynamics and Lasers Conf.*, AIAA, San-Antonio, Texas, Paper 2009–4223 (2009).
8. E. J. Jumper et al., "Airborne aero-optics laboratory," *Opt. Eng.* **52**(7), 071408 (2013).
9. S. Gordeyev and E. J. Jumper, "Fluid dynamics and aero-optics of turrets," *Prog. Aerospace Sci.* **46**(8), 388–400 (2010).
10. S. Abado, S. Gordeyev, and E. J. Jumper, "Approach for two-dimensional velocity mapping," *Opt. Eng.* **52**(7), 071402 (2013).
11. A. Chatterjee, "An introduction to the proper orthogonal decomposition," *Curr. Sci.* **78**(7), 808–817 (2000).
12. D. J. Goorskey, R. Drye, and M. R. Whiteley, "Dynamic modal analysis of transonic Airborne Aero-Optics Laboratory conformal window flight-test aero-optics," *Opt. Eng.* **52**(7), 071414 (2013).
13. S. Gordeyev et al., "Aero-optical environment around a cylindrical turret with a flat window," *AIAA J.* **49**(2), 308–315 (2011).
14. N. De Lucca, S. Gordeyev, and E. J. Jumper, "In-flight aero-optics of turrets," *Opt. Eng.* **52**(7), 071405 (2013).
15. D. J. Tritton, *Physical Fluid Dynamics*, 2nd ed., Oxford University Press, New York (1988).
16. J. P. Siegenthaler, S. Gordeyev, and E. J. Jumper, "Shear layers and aperture effects for aero-optics," in *36th AIAA Plasmadynamics and Lasers Conf.*, AIAA, Toronto, Canada, Paper 2005–4772 (2005).
17. K. Karhunen, "Zur spektraltheorie stochastischer prozesse," *Ann. Acad. Sci. Finnicae Ser. A* **34**, 1–7 (1946).
18. M. M. Loève, *Probability Theory*, Van Nostrand, Princeton, New Jersey (1955).
19. J. L. Lumley, *Stochastic Tools in Turbulence*, Academic Press, New York, NY (1970).
20. K. Mela and J. N. Louie, "Correlation length and fractal dimension interpretation from seismic data using variograms and power spectra," *Geophysics* **66**(5), 1372–1378 (2001).
21. S. Gordeyev, T. Hayden, and E. Jumper, "Aero-optical and flow measurements over a flat-windowed turret," *AIAA J.* **45**(2), 347–357 (2007).
22. T. S. Ross, "Limitations and applicability of the Maréchal approximation," *Appl. Opt.* **48**(10), 1812–1818 (2009).
23. C. Porter, S. Gordeyev, and E. Jumper, "Large-aperture approximation for not-so-large apertures," *Opt. Eng.* **52**(7), 071417 (2013).
24. A. M. Nightingale et al., "Regularizing shear layer for adaptive optics control applications," in *36th AIAA Plasmadynamics and Lasers Conf.*, AIAA, Toronto, Ontario Paper 2005–4774 (2005).
25. A. M. Nightingale et al., "Adaptive-optic correction of a regularized compressible shear layer," in *37th AIAA Plasmadynamics and Lasers Conf.*, AIAA, San Francisco, California Paper 2006–3072 (2006).

Biographies of the authors are not available.